

## HIERARCHICAL TRIGGERING OF STAR FORMATION BY SUPERBUBBLES IN W3/W4

M. S. OEY

Department of Astronomy, 830 Dennison Building, University of Michigan, Ann Arbor, MI 48109-1090

ALAN M. WATSON

Centro de Radioastronomía y Astrofísica, Universidad Nacional Autónoma de México, Apartado Postal 3-72,  
58089 Morelia, Michoacán, México

KATIE KERN<sup>1</sup>

Dept. of Astronomy, University of Wisconsin, 475 Charter St., Madison, WI 53706

GREGORY L. WALTH

Lowell Observatory, 1400 W. Mars Hill Rd., Flagstaff, AZ 86001

*Accepted to the **ASTRONOMICAL JOURNAL** 21 September 2004*

### ABSTRACT

It is generally believed that expanding superbubbles and mechanical feedback from massive stars trigger star formation, because there are numerous examples of superbubbles showing secondary star formation at their edges. However, while these systems show an age sequence, they do not provide strong evidence of a causal relationship. The W3/W4 Galactic star-forming complex suggests a three-generation hierarchy: the supergiant shell structures correspond to the oldest generation; these triggered the formation of IC 1795 in W3, the progenitor of a molecular superbubble; which in turn triggered the current star-forming episodes in the embedded regions W3-North, W3-Main, and W3-OH. We present *UBV* photometry and spectroscopic classifications for IC 1795, which show an age of 3 – 5 Myr. This age is intermediate between the reported 6 – 20 Myr age of the supergiant shell system, and the extremely young ages ( $10^4 - 10^5$  yr) for the embedded knots of ultracompact H II regions, W3-North, W3-Main, and W3-OH. Thus, an age sequence is indeed confirmed for the entire W3/W4 hierarchical system. This therefore provides some of the first convincing evidence that superbubble action and mechanical feedback are indeed a triggering mechanism for star formation.

*Subject headings:* stars: formation — ISM: bubbles — ISM: clouds — ISM: individual (W3, W4) — ISM: structure — open clusters and associations: individual (IC 1795, IC 1805)

### 1. INTRODUCTION

The shocks in expanding superbubbles and supernova remnants are widely believed to be a primary mechanism for triggering star formation. Although this mechanical feedback from massive stars cannot be the only catalyst for the gravitational collapse of molecular clouds, there are numerous examples of superbubbles that show young, star-forming regions at their edges. In the Large Magellanic Cloud, superbubble systems like N11 (Walborn & Parker 1992), N44 (Oey & Massey 1995), and N51 D (Oey & Smedley 1998) all show young OB associations, typically with ages  $\lesssim 3$  Myr, on the outer edges of the shells, while associations that are somewhat older, typically by a few Myr, are responsible for the formation of the shells themselves.

However, it is important to distinguish between *sequential* star formation and *triggered* star formation. Studies of the stellar populations in systems like the above examples conclusively demonstrate that the star formation is sequential, but it is much more difficult to demonstrate a causal relationship. For any star formation that takes place in two adjacent molecular clouds, or even subregions of the same cloud, if the superbubble from the older region grows to impact the younger region, the resulting configuration will show a younger nodule on the edge of an older one. Thus, although they are suggestive of triggering, two-

generation systems do not constitute strong evidence that it is actually taking place.

On the other hand, a hierarchical system of three or more generations would provide much stronger evidence of a causal relationship. An example of superbubble-triggered star formation over three generations should show the oldest shell with a younger superbubble at its edge, which in turn shows even younger star formation on its edge. Such a scenario is extremely unlikely to be coincidental, sequential star formation. In what follows, we identify the W3/W4 Galactic star-forming complex as the first example of three-generation, hierarchical triggered star formation. Thus this offers much more concrete support for the widely-held view that superbubble expansion triggers star formation.

### 2. THE W3/W4 COMPLEX

The W3/W4 complex is located in the Perseus arm of the Galaxy, at a distance of about 2.3 kpc (Massey et al. 1995a). W4 shows a nebular shell roughly  $1^\circ$  in diameter, and it is also at the base of the well-known Perseus “chimney” that is seen in H I (Normandeau et al. 1996). Dennison et al. (1997) find that the “chimney” is the lower section of an elongated, but closed, shell that extends  $\sim 230$  pc above the Galactic plane and is visible in H $\alpha$  (Figure 1). Most recently, Reynolds et al. (2001)

<sup>1</sup>Participant in the 2003 Research Experience for Undergraduates Program, Northern Arizona University.

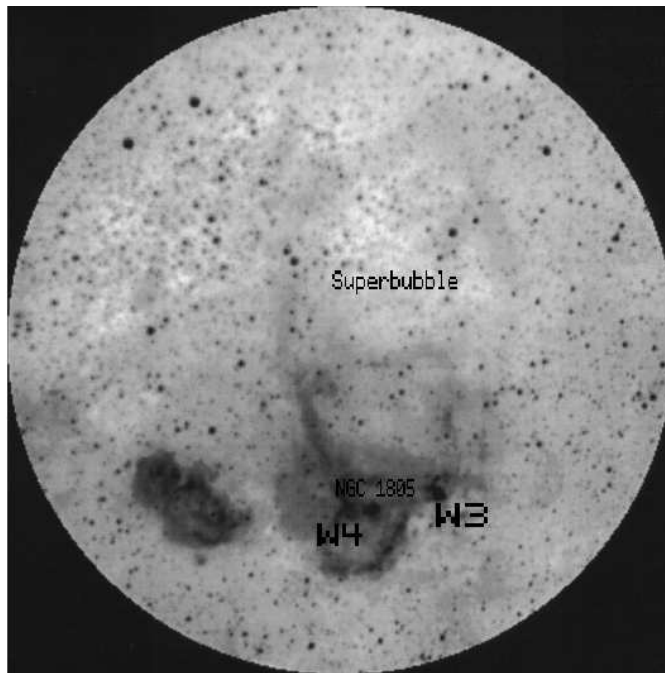


FIG. 1.—  $H\alpha$  image of the  $\sim 1300$ -pc superbubble that is blowing out above the Galactic plane from the W4 region (image from Dennison et al. 1997).

FIG. 2.— Grayscale of the W3 region from the DSS, overlaid by CO contours from the FCRAO CO survey. [Figure available as JPEG on the astro-ph submission.]

identify an even larger loop that is  $\sim 1300$  kpc above the Galactic plane, of which the Dennison et al. superbubble is the lower section. For all of these shell features, the W4 region is located at the Galactic plane apex. At the center of the W4 shell is the OB association IC 1805.

W3 (Figure 2) is a smaller H II region,  $\sim 30'$  (20 pc) in diameter, on the northwest edge of the W4 shell. As a thermal radio source, W3 subdivides into a complex with three dominant knots of ultracompact H II regions: W3-Main, W3-North, and W3-OH. As seen in Figure 2, these knots are embedded in a shell of molecular gas that surrounds the OB association IC 1795. The young, continuum radio-emitting cluster NGC 896 is seen against the western edge of the CO shell.

The configuration of the larger Perseus chimney/superbubble and smaller IC 1795/W3 superbubble are strongly suggestive of a three-generation system of hierarchical triggered star formation. That scenario would imply that the Perseus chimney/superbubble, formed by the first generation, triggered the formation of IC 1795 as the second generation, and its superbubble in turn triggered the W3 embedded star-forming regions W3-Main, W3-North, and W3-OH, thereby constituting the third generation. If this model is correct, it should be reflected by a corresponding age sequence. In this study, we evaluate the ages of the associated stellar populations for these three putative generations, based on both new data for IC 1795 and studies in the literature.

### 3. IC 1795

Since IC 1795 represents the intermediate, second generation of stars in the complex, strong constraints on its age are necessary to test the model of hierarchical trigger-

ing of star formation. To date, the only published studies of the stellar population in IC 1795 are based on photographic and photoelectric studies by Ogura & Ishida (1976) and Sato (1970). We have therefore carried out a new investigation based on modern CCD photometry and spectroscopic observations. While our intent was to examine IC 1795 in detail, we also obtained stellar data for the wider W3 region shown in Figure 3; these data are presented in the Appendix.

#### 3.1. Photometric observations

*UBV* imaging was obtained on 1999 October 6–9 at the 84-cm telescope of the Observatorio Astronómico Nacional at San Pedro Mártir (SPM), Baja California Norte, México. We used a  $1024 \times 1024$  SITe CCD binned  $2 \times 2$ , which gave  $0.85''$  pixels and an instantaneous field of view of  $7' \times 7'$ . The seeing was typically around  $2''$  and the sky was clear. IC 1795 was imaged in four pointings, with BD +61 411 in each corner of the CCD. NGC 896 and W3-Main were imaged in one pointing each, and W3-North was imaged in three pointings. Our *U*-band mosaic of the entire region is shown in Figure 3. At each pointing, we obtained exposures of 600 seconds in *V*, 900 seconds in *B*, and 1200 seconds in *U*, along with shorter 10 and 100 second images in each filter. Each image was corrected for bias offset and was then divided by a twilight flat field. Variance between the flat fields obtained each nights and direct measurements of a grid stars suggest that the flat fields are good to about 0.5% rms.

We observed roughly 15 Landolt (1983) standards each night over a range of airmass and color. Instrumental magnitudes were determined by synthetic aperture photometry with a  $17''$  star aperture and a sky annulus with inner and

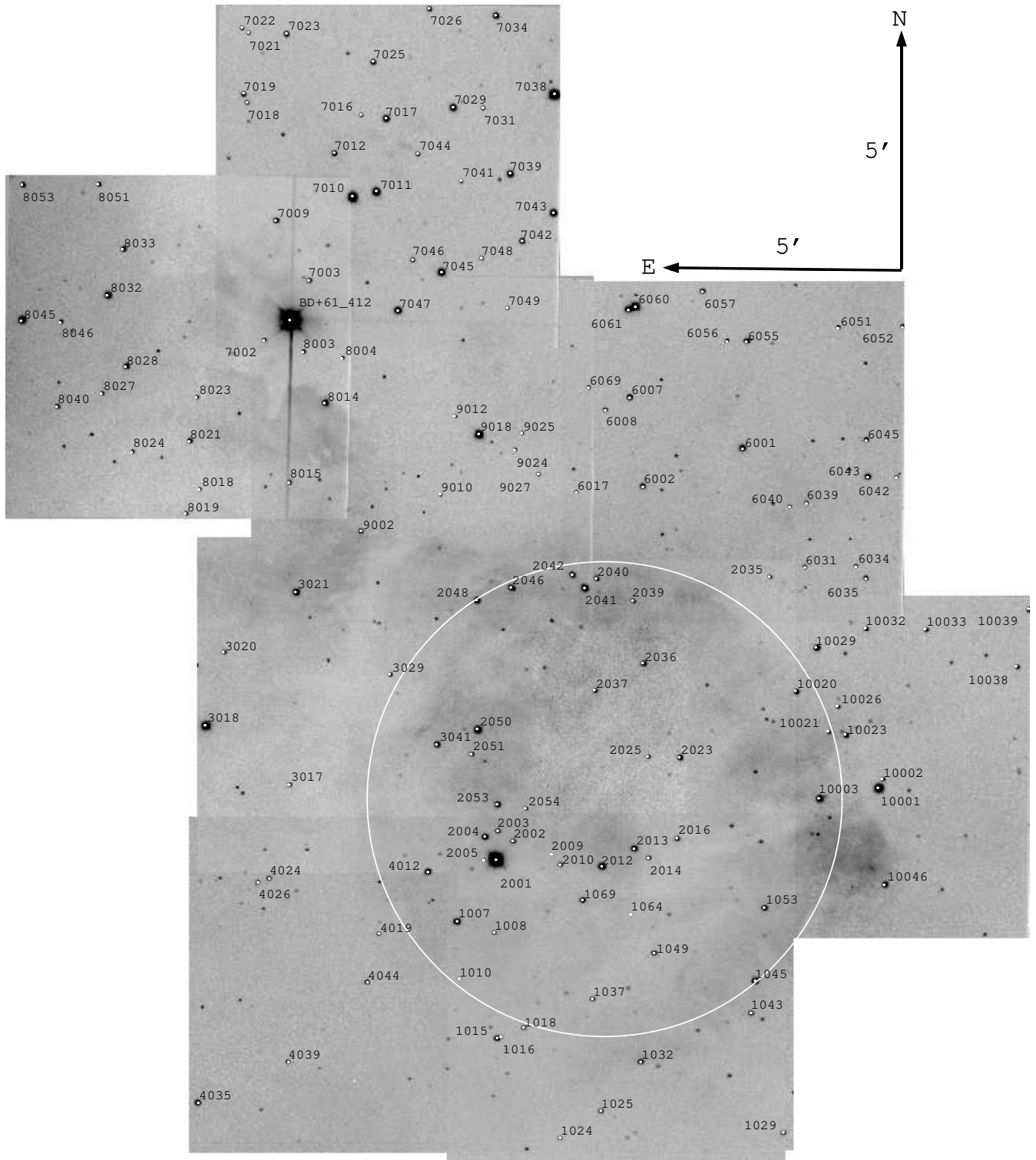


FIG. 3.—  $U$ -band mosaic of the W3 region, with stars having new  $U$ -band photometry identified, for  $U < 18$ . The circle shows the IC 1795 region for which the H-R diagram was constructed.

outer diameters of  $34''$  and  $51''$ . We determined the transformation between the instrumental and standard systems by fitting all of the  $\sim 60$  observations simultaneously, with a separate linear extinction coefficient for each night, but a single set of color coefficients and zero points. Linear color transformations were adequate for  $B$  and  $V$ , but the data required a quadratic color transformation for  $U$ . The RMS residuals were 2.1% in  $U$  and 1.5% in  $B$  and  $V$ .

We selected stars by eye in each 600 second  $V$  image, as these were by far the deepest images. We then performed synthetic aperture photometry on each image using an  $8.5''$  diameter star aperture and a sky annulus with inner and outer diameters of  $34''$  and  $51''$ . Aperture corrections between  $8.5''$  and  $17''$  diameter apertures were determined for each image. We then calculated the standard magnitude for each star and its uncertainty, taking into account read noise and photon noise in the star and sky apertures, flat-field uncertainties, and transformation uncertainties. Since we had three (10 second, 100 second, and 600/900/1200 second) images in each band, we selected the unsaturated measurement with the lowest uncertainty. Our complete set of new  $UBV$  photometry is presented in the Appendix, Table 2.

We compared our data with photometry reported by Ogura & Ishida (1976) and Sato (1970). The Ogura & Ishida measurements are mostly based on iris photometry of photographic plates, calibrated to a subset of photoelectric data, while those of Sato are photoelectric. Figure 4 shows the comparison of our modern data to these earlier studies. There is a large scatter in the photometric differences for both, with a large systematic pattern seen in the comparison to the data of Ogura & Ishida as function of magnitude. The differences cannot be explained with the published information. One might suspect a non-linearity in the detector, but thorough annual ‘‘health checks’’ of this CCD performed every year since 2000 have failed to find any evidence for such a problem. We note that Figure 4 shows that the photometry from these previous studies also appear to be inconsistent with each other.

### 3.2. Spectroscopic observations

Spectroscopic observations of candidates for the earliest-type stars were obtained with the 2.1-m telescope at SPM during the nights of 1999 October 15 – 17. We used the 600 line  $\text{mm}^{-1}$  grating on the Boller & Chivens spectrograph and Thomson  $2048 \times 2048$  CCD, yielding a useable wavelength coverage of about  $3500 - 5900 \text{ \AA}$  at spatial and spectral resolutions of about  $3 \text{ \AA}$  and  $1.3'' \text{ px}^{-1}$ , respectively. The stars observed spectroscopically were selected from the wider region around IC 1795, not just in the central region that we imaged in  $UBV$ . The spectroscopic candidates were the bluest by their reddening-free  $Q$  values ( $Q \lesssim -0.3$ ) and brightest ( $V \lesssim 15$ ) as reported by Ogura & Ishida (1976) and Sato (1970).

The spectroscopic data were reduced with the IRAF<sup>2</sup> software. The raw data were bias-subtracted and then flat-fielded using the quartz lamp calibration images. Owing to a problem with the sky frames, an illumination correction was only applied to data taken on 1999 October 15. During aperture extraction, the local background was evaluated for every set of 10 rows in the chip and subtracted;

since this was straightforward, the lack of an explicit illumination correction is considered unimportant. The spectra were extracted following standard procedures by fitting the trace along the dispersion and applying wavelength calibrations from He-Ne-Ar arc lamp observations taken during each night.

The twenty stars with spectroscopic observations were independently classified by KK and MSO, with agreement generally within one spectral subtype, and differences resolved upon reinspection. O and early B-type stars were classified according to the criteria of Walborn & Fitzpatrick (1990). Our observations of spectroscopic standards aided in classifying the stars.

### 3.3. H-R Diagram

We focused on the stellar population of IC 1795, taken to be the stars within a  $5'$ -radius, circular region centered at  $02^{\text{h}}26^{\text{m}}15.^{\text{s}}0, +62^{\circ}02'00.''0$  (J2000.0) (Figure 3). The stellar effective temperatures  $T_{\text{eff}}$  and bolometric corrections (BCs) were estimated for the stars with spectral classifications using the calibrations of Chlebowski & Garmany (1991) for O stars and Humphreys & McElroy (1984) for B stars. For the dominant, bright star BD +61 411 (ID number 2001 = OI 89) we adopt spectral type O6.5 V((f)) from Mathys (1989). For blue stars (reddening-corrected  $B - V < -0.22$  or  $Q < -0.6$ ) without direct spectroscopic classifications, but having good photometry with formal errors in  $V$ ,  $B - V$ , and  $U - B$  less than 0.03, 0.05, and 0.05, respectively, we estimated  $\log T_{\text{eff}}$  from the reddening-free parameter  $Q = (U - B) - 0.72(B - V)$  using the relations of Massey et al. (1995b). These authors also derive a relation between the BC and  $\log T_{\text{eff}}$ , which we then used to obtain the BCs for these stars. The remaining stars have poorer photometry, and for these we estimated  $\log T_{\text{eff}}$  using only the reddening-corrected  $(B - V)_0$ , from the relation also given by Massey et al. (1995b). We used a fixed value for the color excess of  $E(B - V) = 1.25$ , which is the median value for the stars with spectroscopic classifications. The same relation between BC and  $\log T_{\text{eff}}$  was then applied to obtain the bolometric corrections.

With the bolometric corrections in hand, we then computed the bolometric magnitudes, as usual correcting for extinction and distance, as  $M_{\text{bol}} = V - A_V + \text{BC} + \text{DM}$ . Hanson & Clayton (1993) determine  $A_V = 2.9 E(B - V)$  for the neighboring region IC 1805, so we adopt this relation between the total to selective extinction. Likewise, we adopt the distance modulus  $\text{DM} = 11.85$  (2.3 kpc) derived by Massey et al. (1995a) for IC 1805, a value consistent with the distance adopted in past studies of the W3 complex.

Figures 5a and b show the  $B - V$  vs  $V$  and  $U - B$  vs  $V$  color-magnitude diagrams for IC 1795, respectively, while Figure 6 shows the resulting  $M_{\text{bol}}$  vs  $T_{\text{eff}}$  H-R diagram. Stars 1053 (OI 42), 2004 (OI 86), and 10003 (OI 40) were omitted since their spectral types revealed them to be foreground F and G dwarfs. Solid symbols represent stars placed on the basis of spectroscopic classifications; asterisks represent the stars with good photometry that are placed by their  $Q$  values; and crosses represent the remainder of the data, placed by their  $(B - V)_0$  colors alone. Isochrones for 3, 4, and 5 Myr are overplotted in Figure 6,

<sup>2</sup>IRAF is distributed by NOAO, which is operated by AURA, Inc., under cooperative agreement with the NSF.

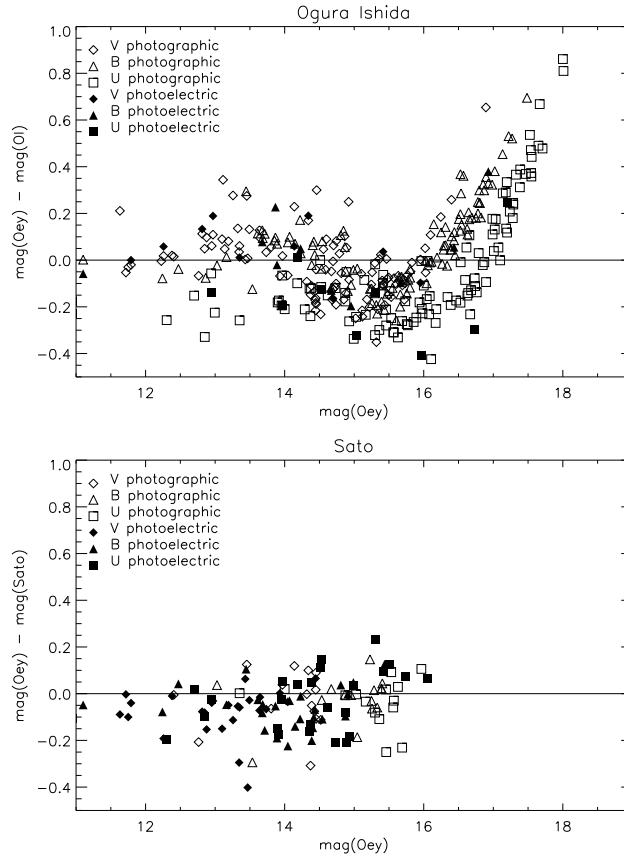


FIG. 4.— Photometric differences of our photometry with those of Ogura & Ishida (1976; top) and Sato (1970; bottom), as a function of magnitude.

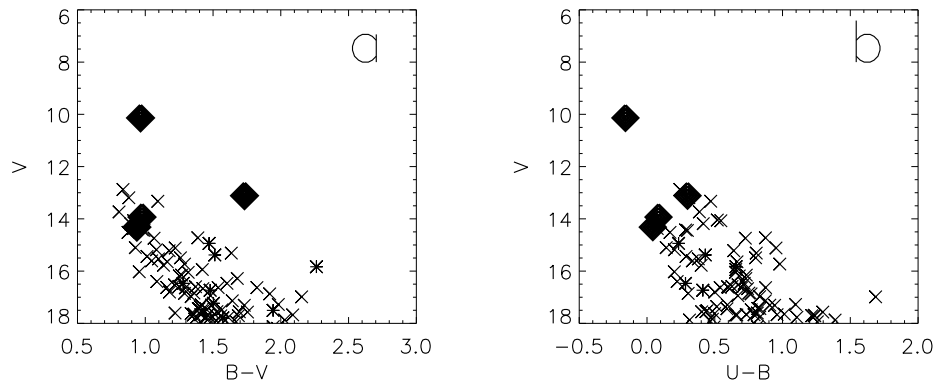


FIG. 5.— Color-magnitude diagrams for IC 1795. Solid symbols and asterisks show, respectively, stars with spectroscopic classifications and reliable reddening-free  $Q$  values; crosses show the remainder, lower-quality data (see text). Star 3041 (OI 109; the second-brightest star) is heavily reddened and appears displaced relative to the locus of the other stars.

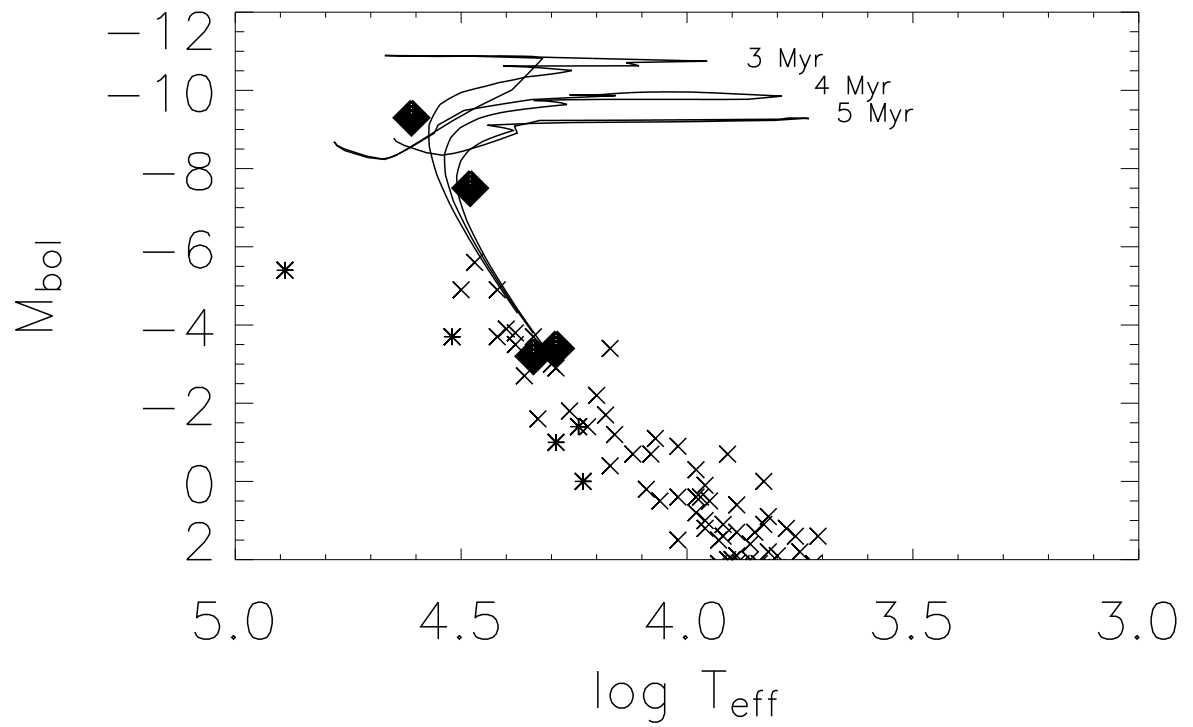


FIG. 6.— H-R diagram for IC 1795. Solid, asterisk, and cross symbols show stars with  $T_{\text{eff}}$  and  $M_{\text{bol}}$  estimated from, respectively, spectroscopic classifications, reddening-free  $Q$  values, and  $(B - V)_0$  only. Isochrones for 3, 4, and 5 Myr from Schaller et al. (1992) are overplotted as labeled.

from Schaller et al. (1992) for solar metallicity. From Figure 6, we infer an age of 3 – 5 Myr for IC 1795. Data for the individual stars in IC 1795 are presented in Table 1: The first two columns give ID numbers assigned by this work and Ogura & Ishida (1976), respectively, columns 3 and 4 give the celestial coordinates for epoch J2000.0, and columns 5 – 10 list the  $V$ ,  $B$ , and  $U$  magnitudes with corresponding formal (non-systematic) uncertainties. Column 11 gives our spectral classification for stars that were observed spectroscopically.

#### 4. DISCUSSION AND CONCLUSION

We now return to the question of hierarchical triggered star formation in the entire W3/W4 complex.

The age of the 230-pc Perseus chimney/superbubble feature is somewhat problematic. Dennison et al. (1997) roughly estimate it to be 6 – 10 Myr old, while Basu et al. (1999) find a much younger age of  $\sim 2.5$  Myr, from a more detailed semi-analytic investigation. Basu et al. solve simultaneously for the age and scale height of the ambient gas, and it is important to note that this young age estimate is largely due to the surprisingly small, 25-pc, Galactic scale height of the ambient gas that they find. Reynolds et al. (2001) argue that the largest, 1300-pc loop associated with the region requires at least 10 – 20 Myr to form.

The stellar population at the center of W4, at the apex of the chimney/superbubble system, is extremely young. The central OB association, IC 1805, is around 1 – 3 Myr old, as determined by Massey et al. (1995a) from a detailed study including spectral classifications of the earliest-type stars. This age is consistent with that determined for the wider population, Cas OB6 / OCl 352 (e.g., Normandeau et al. 1996; Mathys 1987; Llorente de Andr es et al. 1982).

Dennison et al. (1997) suggest that an earlier generation of star formation, preceding the birth of IC 1805, was responsible for forming the 230-pc Perseus superbubble. Indeed, Carpenter et al. (2000) independently suggest the existence of an older star-forming episode to explain the large number and distribution of molecular cloudlets and globules scattered in the wider W4 area. They speculate that these molecular globules are the remnants of a giant molecular cloud that was dispersed by the photodissociation, stellar winds, and supernovae of the resulting star-forming region.

IC 1805, at the center of W4, represents a more recent generation. The young, 1 – 3 Myr age found by Basu et al. (1999) for the Dennison superbubble is consistent with the age of IC 1805, suggesting that this association is responsible for that shell. The unusually small scale height that is linked to this young age by Basu et al. is also beautifully consistent with the existence of an ear-

lier generation and earlier superbubble in the same region, which would have cleared out much of the ambient ISM, in particular across Galactic latitude. This naturally points to the larger, 1300-pc shell reported by Reynolds et al. (2001), that they estimate to be 10 – 20 Myr old. Note that if a normal ISM scale height is assumed, the age of the Dennison superbubble would be older, around 6 – 10 Myr old, as estimated by those authors, regardless of the age of IC 1805. Thus, it is a fairly robust result that the superbubble activity associated with W4 is at least 6 – 20 Myr old.

From Figure 6, we derived an age for IC 1795, in the center of the W3 superbubble, of 3 – 5 Myr. This age is consistent with the location of IC 1795 in the central, cleared area of the molecular shell (Figure 2), while younger, ongoing star formation, is taking place in the ultracompact H II regions on the edge of that shell, in W3-North, W3-Main, and W3-OH. These youngest star-forming regions show individual sources embedded in their molecular gas cores, which are of order  $10^4$  to  $10^5$  years old (e.g. Megeath et al. 1996; Tieftrunk et al. 1998). Therefore, the entire W3/W4 complex does indeed show an age sequence consistent with hierarchical triggering of star formation: The first generation corresponds to the 1300 pc loop, and possibly the Perseus superbubble, along with the progenitor stellar population; these triggered the formation of IC 1795 on the western edge; which in turn triggered the formation of W3-North, W3-Main, and W3-OH at the edges of its shell (Figures 1–2). IC 1805, at the apex of the W4 shells by projection, is a young, 1 – 3 Myr old association that appears not to be responsible for triggering the creation of IC 1795. It is possible that the formation of IC 1805 was itself triggered by the earliest generation, and possibly it, too, is located on the edge of the shell, although projected toward the center in our line of sight.

In contrast to two-generation superbubble systems, this three-generation configuration is extremely difficult to attribute to coincidental sequential star formation. Thus, the W3/W4 complex provides some of the strongest evidence to date that superbubble activity and mechanical feedback from massive stars is indeed a mechanism for triggering star formation. Additional examples of confirmed multi-generation star formation can further confirm this.

We thank Phil Massey for discussions on the photometry, and Brian Skiff for cross-referencing the stars in the literature. MSO and GLW acknowledge support from the National Science Foundation, grant AST-0204853. KK participated through the Research Experience for Undergraduates program at Northern Arizona University, also supported by the National Science Foundation. Much of this work was done by MSO at the Space Telescope Science Institute and Lowell Observatory.

#### REFERENCES

- Basu, S., Johnstone, D., & Martin, P. G. 1999, *ApJ*, 516, 843  
 Carpenter, J. M., Heyer, M. H., & Snell, R. L. 2000, *ApJS*, 130, 381  
 Chlebowksi, T. & Garmany, C. D. 1991, *ApJ*, 368, 241  
 Dennison, B., Topasna, G. A., & Simonetti, J. H. 1997, *ApJ*, 474, L31  
 Hanson, M. M. & Clayton, G. C. 1993, *AJ*, 106, 1947  
 Humphreys, R. M. & McElroy, D. B. 1984, *ApJ*, 284, 565  
 Llorente de Andr es, F., Burk ı, G., & Ruiz de Arbol, J. A. 1982, *A&A*, 107, 43  
 Massey, P., Johnson, K. E., & DeGioia-Eastwood, K. 1995, *ApJ*, 454, 151  
 Massey, P., Lang, C. C., Degioia-Eastwood, K., & Garmany, C. D. 1995, *ApJ*, 438, 188  
 Mathys, G. 1987, *A&AS*, 71, 201  
 Mathys, G. 1989, *A&AS*, 81, 237  
 Megeath, S. T., Herter, T., Beichman, C., Gautier, N., Hester, J. J., Rayner, J., & Shupe, D. 1996, *A&A*, 307, 775

TABLE 1  
PHOTOMETRY AND SPECTRAL TYPES FOR IC 1795

ID	OI	RA(J2000.0)	Dec(J2000.0)	$V$	$V$ err	$B$	$B$ err	$U$	$U$ err	Sp Type
1007	112	02:26:41.31	+61:59:24.2	14.318	0.001	15.256	0.001	15.299	0.002	B1-2 V
1008	...	02:26:34.63	+61:59:10.6	15.312	0.001	16.947	0.003	17.753	0.011	...
1009	...	02:26:38.45	+61:59:26.2	18.138	0.013	19.585	0.028	20.080	0.120	...
1010 <sup>a</sup>	...	02:26:40.83	+61:58:11.7	17.233	0.005	18.736	0.011	18.000	0.023	...
1011	...	02:26:34.54	+61:58:16.6	18.124	0.013	20.069	0.042	20.883	0.235	...
1034	...	02:26:26.63	+61:57:41.9	17.292	0.006	18.705	0.013	19.298	0.055	...
1035	...	02:26:27.21	+61:58:14.4	17.278	0.006	19.260	0.018	20.356	0.147	...
1036	...	02:26:21.67	+61:57:55.0	16.840	0.004	18.199	0.008	18.951	0.039	...
1037	...	02:26:16.89	+61:57:47.9	15.778	0.002	16.913	0.004	17.313	0.010	...
1038	...	02:26:17.89	+61:57:25.3	17.691	0.008	19.148	0.018	20.382	0.150	...
1039	...	02:26:09.30	+61:57:32.1	17.434	0.006	18.826	0.013	19.659	0.073	...
1040	...	02:26:10.50	+61:58:02.0	16.733	0.004	18.212	0.008	18.624	0.030	...
1045	...	02:25:47.67	+61:58:12.6	14.184	0.001	15.076	0.001	15.491	0.003	...
1046	...	02:25:56.53	+61:58:01.9	17.430	0.006	18.875	0.014	19.693	0.083	...
1047	...	02:26:00.88	+61:58:15.9	17.550	0.008	19.079	0.019	19.514	0.075	...
1048	...	02:26:04.52	+61:58:26.8	16.986	0.006	19.140	0.020	20.827	0.254	...
1049	...	02:26:05.86	+61:58:46.6	14.939	0.001	16.410	0.002	16.643	0.006	...
1050	...	02:26:07.08	+61:58:41.7	17.712	0.008	19.269	0.019	20.507	0.163	...
1051	...	02:25:58.48	+61:58:49.5	17.481	0.008	19.047	0.019	19.816	0.095	...
1052	...	02:25:46.07	+61:59:10.6	17.624	0.008	18.963	0.017	19.462	0.072	...
1053 <sup>b</sup>	42	02:25:46.12	+61:59:45.2	14.447	0.001	15.602	0.001	16.180	0.004	G3 V
1054	...	02:25:51.04	+61:59:54.3	16.872	0.004	18.790	0.012	19.558	0.062	...
1059	...	02:25:59.35	+62:01:09.4	18.190	0.021	20.167	0.058	22.365	1.224	...
1061	...	02:26:03.27	+61:59:36.1	16.641	0.004	17.937	0.007	18.635	0.031	...
1062	...	02:26:04.96	+61:59:40.1	17.873	0.010	19.902	0.034	21.290	0.348	...
1063	...	02:26:06.20	+61:59:19.2	17.871	0.010	19.329	0.022	19.643	0.076	...
1064 <sup>a</sup>	...	02:26:10.09	+61:59:35.0	17.791	0.009	19.363	0.022	16.960	0.015	...
1065	...	02:26:05.55	+62:00:30.0	17.940	0.014	19.610	0.031	20.867	0.226	...
1069	92	02:26:18.80	+61:59:52.9	15.182	0.001	16.264	0.002	16.467	0.005	...
1070	...	02:26:25.07	+61:59:38.4	17.362	0.007	18.768	0.014	19.283	0.055	...
2001	89	02:26:34.41	+62:00:42.6	10.137	0.000	11.102	0.001	10.943	0.000	O6.5 V((f)) <sup>c</sup>
2002	87	02:26:31.43	+62:01:06.7	15.532	0.002	16.630	0.003	17.009	0.007	...
2003	85	02:26:34.15	+62:01:19.3	14.725	0.001	16.113	0.001	16.987	0.005	...
2004 <sup>b</sup>	86	02:26:36.47	+62:01:11.9	13.968	0.001	15.044	0.001	15.458	0.002	F8 V
2005 <sup>a</sup>	...	02:26:36.64	+62:00:41.8	16.285	0.005	16.098	0.002	13.596	0.002	...
2006	...	02:26:38.83	+62:00:30.4	16.470	0.003	18.073	0.007	18.791	0.028	...
2007	...	02:26:29.62	+62:00:19.1	17.768	0.011	19.380	0.021	20.486	0.146	...
2008	...	02:26:26.17	+62:00:32.5	17.708	0.012	19.395	0.028	20.611	0.174	...
2009 <sup>a</sup>	...	02:26:24.43	+62:00:50.3	17.504	0.008	19.447	0.024	16.589	0.015	...
2010	90	02:26:22.89	+62:00:37.1	15.383	0.002	16.896	0.003	17.326	0.009	...
2012	91	02:26:15.37	+62:00:35.7	13.734	0.001	14.541	0.001	14.928	0.002	...
2013	60	02:26:09.59	+62:00:58.3	14.425	0.001	15.404	0.001	15.689	0.003	...
2014	61	02:26:07.00	+62:00:46.8	15.115	0.002	16.336	0.003	17.288	0.011	...
2016	59	02:26:01.91	+62:01:12.2	15.438	0.001	16.451	0.002	16.739	0.005	...
2017	...	02:25:52.29	+62:00:09.9	17.441	0.005	18.837	0.011	19.427	0.047	...
2019	...	02:25:46.88	+62:01:09.2	16.185	0.002	17.437	0.004	18.118	0.016	...
2020	...	02:25:49.17	+62:01:17.5	17.661	0.008	19.176	0.017	19.909	0.083	...
2021	...	02:25:52.16	+62:01:28.9	15.939	0.002	17.360	0.003	18.015	0.015	...
2022	58	02:25:48.01	+62:02:37.5	15.731	0.002	17.021	0.004	18.001	0.021	...
2023	57	02:26:01.55	+62:02:54.5	14.518	0.001	15.391	0.002	15.561	0.004	...
2024	...	02:26:03.49	+62:02:32.5	16.976	0.007	18.315	0.014	19.146	0.067	...
2025	56	02:26:07.28	+62:02:55.2	15.643	0.003	16.805	0.005	17.469	0.016	...
2026	...	02:26:03.63	+62:03:26.1	17.513	0.011	18.928	0.023	19.371	0.082	...
2027	...	02:25:55.83	+62:03:29.3	17.673	0.008	19.083	0.017	19.873	0.097	...
2028	...	02:25:44.84	+62:03:41.8	15.834	0.003	18.097	0.009	18.754	0.039	...
2029	...	02:25:46.06	+62:03:45.0	16.802	0.005	17.981	0.007	18.481	0.030	...
2030	...	02:25:46.67	+62:03:57.5	16.670	0.004	18.095	0.008	18.837	0.037	...
2032	...	02:25:56.82	+62:04:27.5	16.624	0.004	17.783	0.006	18.383	0.026	...
2033	...	02:25:47.13	+62:05:21.1	17.303	0.005	18.792	0.013	19.698	0.091	...
2036	55	02:26:08.24	+62:04:53.4	14.445	0.001	15.436	0.002	15.734	0.005	...
2037	81	02:26:16.94	+62:04:18.6	15.608	0.003	16.655	0.004	16.990	0.013	...
2038	...	02:26:15.59	+62:02:41.4	17.766	0.014	19.218	0.033	20.049	0.157	...
2039	54	02:26:10.11	+62:06:12.3	16.027	0.002	16.983	0.004	17.185	0.010	...
2040	76	02:26:16.75	+62:06:39.9	14.740	0.001	15.805	0.002	16.531	0.006	...
2041	77	02:26:18.83	+62:06:27.7	13.191	0.001	14.070	0.001	14.379	0.001	...
2042	75	02:26:21.09	+62:06:44.3	14.045	0.001	14.988	0.001	15.507	0.002	...
2043	...	02:26:19.58	+62:05:40.0	16.598	0.005	17.969	0.010	18.564	0.049	...
2044	...	02:26:24.79	+62:05:46.8	16.049	0.002	17.366	0.005	18.019	0.019	...
2045	...	02:26:26.14	+62:04:47.1	16.527	0.005	17.744	0.009	18.416	0.038	...
2046	...	02:26:32.12	+62:06:27.4	14.074	0.001	14.989	0.001	15.534	0.002	...
2048	80	02:26:38.29	+62:06:11.1	13.326	0.001	14.419	0.001	14.889	0.002	...
2049	...	02:26:33.69	+62:05:34.9	16.589	0.003	17.838	0.007	18.465	0.032	...
2050	82	02:26:38.01	+62:03:27.9	12.877	0.001	13.713	0.002	13.956	0.001	...
2051	110	02:26:39.03	+62:02:55.9	15.219	0.001	16.395	0.003	17.035	0.009	...
2052	...	02:26:36.70	+62:02:47.0	16.283	0.003	17.962	0.007	18.691	0.032	...
2053	83	02:26:34.32	+62:01:52.8	14.372	0.001	15.285	0.001	15.361	0.003	...
2054	84	02:26:29.22	+62:01:48.1	15.491	0.002	16.751	0.003	17.552	0.013	...
2055	...	02:26:26.89	+62:02:48.4	17.646	0.017	19.006	0.034	20.019	0.170	...
2056	...	02:26:40.58	+62:02:10.4	17.309	0.009	19.040	0.024	19.982	0.125	...



TABLE 1, *continued*

ID	OI	RA(J2000.0)	Dec(J2000.0)	$V$	$V$ err	$B$	$B$ err	$U$	$U$ err	Sp Type
3007	...	02:26:44.60	+62:00:48.0	16.942	0.005	18.424	0.011	19.095	0.042	...
3009	...	02:26:47.81	+62:01:06.9	17.568	0.006	19.322	0.019	20.619	0.167	...
3010	...	02:26:50.89	+62:00:45.5	17.136	0.005	18.778	0.013	19.651	0.066	...
3030	...	02:26:52.69	+62:04:11.9	17.669	0.012	19.132	0.026	20.092	0.141	...
3041	109	02:26:45.29	+62:03:07.6	13.114	0.002	14.846	0.001	15.145	0.003	O9.7 Ia
3043	...	02:26:50.85	+62:02:53.4	17.559	0.011	19.253	0.029	19.657	0.100	...
3044	...	02:26:51.92	+62:02:28.0	17.680	0.011	19.035	0.023	19.698	0.100	...
4010	...	02:26:45.69	+61:59:50.8	16.632	0.004	18.170	0.010	18.710	0.040	...
4011	...	02:26:46.41	+61:59:47.3	16.631	0.004	18.455	0.013	19.330	0.068	...
4012	111	02:26:46.66	+62:00:26.1	13.932	0.002	14.908	0.001	14.993	0.003	B2 V
4060	...	02:26:41.75	+61:58:50.6	17.677	0.008	19.765	0.030	20.418	0.139	...
5009	...	02:26:37.65	+61:59:19.2	18.613	0.030	20.592	0.094	21.002	0.362	...
5014	...	02:26:34.86	+61:57:56.0	18.397	0.019	20.946	0.110	22.188	0.966	...
5037	...	02:26:23.36	+61:58:11.7	18.708	0.025	20.598	0.083	21.881	0.762	...
5041	...	02:26:20.48	+61:57:17.8	18.520	0.021	20.145	0.056	20.943	0.302	...
5069	...	02:25:59.03	+61:59:47.7	17.903	0.011	19.428	0.024	19.893	0.095	...
6020	...	02:26:22.87	+62:06:25.9	17.840	0.012	19.204	0.025	19.687	0.099	...
6024	...	02:26:16.28	+62:06:22.3	17.606	0.012	18.826	0.022	19.640	0.133	...
9039	...	02:26:26.38	+62:06:17.3	18.350	0.018	19.594	0.039	19.897	0.151	...
10003 <sup>b</sup>	40	02:25:36.38	+62:02:04.1	13.100	0.002	14.222	0.001	14.510	0.002	G3 V
10004	...	02:25:34.59	+62:01:40.1	16.471	0.011	17.751	0.018	18.035	0.045	...
10005	...	02:25:36.70	+62:01:18.9	16.153	0.007	17.421	0.012	18.154	0.042	...
10006	...	02:25:37.75	+62:01:19.1	16.853	0.016	18.143	0.024	18.447	0.060	...
10020	33	02:25:40.67	+62:04:19.8	15.102	0.002	16.029	0.003	16.171	0.006	...
10021	35	02:25:34.79	+62:03:28.9	16.399	0.006	17.485	0.009	17.708	0.025	...

<sup>a</sup>Photometry suspect, yielding unphysical parameters; star omitted from analysis.

<sup>b</sup>Foreground star.

<sup>c</sup>Spectral type from Mathys (1989).

Normandeau, M., Taylor, A. R., & Dewdney, P. E. 1996, *Nature*, 380, 687  
Oey, M. S. & Massey, P. 1995, *ApJ*, 452, 210  
Oey, M. S. & Smedley, S. A. 1998, *AJ*, 116, 1263  
Ogura, K. & Ishida, K. 1976, *PASJ*, 28, 651  
Reynolds, R. J., Sterling, N. C., & Haffner, L. M. 2001, *ApJ*, 558, L101

Sato, F. 1970, *Ann. Tokyo Astron. Obs.*, 2nd Ser., 12, 34  
Schaller, G., Schaerer, D., Meynet, G., & Maeder, A. 1992, *A&AS*, 96, 269  
Tieftrunk, A. R., Megeath, S. T., Wilson, T. L., & Rayner, J. T. 1998, *A&A*, 336, 991  
Walborn, N. R. & Fitzpatrick, E. L. 1990, *PASP*, 102, 379  
Walborn, N. R. & Parker, J. W. 1992, *ApJ*, 399, L87

## APPENDIX

Here we present the complete, new stellar dataset for the greater W3 region. Table 2 presents our  $UBV$  photometry for stars observed in the region covered by Figure 3. (The complete version of Table 2 is available in the on-line edition). The first two columns give ID numbers assigned by this work and Ogura & Ishida (1976), respectively, columns 3 and 4 give the celestial coordinates for epoch J2000.0, and columns 5 – 10 list the  $V$ ,  $B$ , and  $U$  magnitudes with corresponding formal (non-systematic) uncertainties. Finally, column 11 gives the number of observations that were averaged to obtain the final values, and column 12 gives the spectral classification resulting from our spectroscopic data.

### *Special notes:*

Star 2001 (OI 89 = BD +61 411): Formal uncertainties  $< 0.001$  in all three bands. This star was classified as O6.5 V((f)) by Mathys (1989).

Star 9018 (OI 71):  $V$  measurement saturated; listed value is adopted from Ogura & Ishida (1976).

Star 2046: Resolved into two stars, OI 78 and OI 79, by Ogura & Ishida (1976).

TABLE 2  
PHOTOMETRY AND SPECTRAL TYPES FOR THE W3 REGION

ID	OI	RA(J2000.0)	Dec(J2000.0)	$V$	$V$ err	$B$	$B$ err	$U$	$U$ err	n-obs	Sp Type
1007	112	2:26:41.31	61:59:24.2	14.318	0.001	15.256	0.001	15.299	0.002	3	B1-2 V
1008	...	2:26:34.63	61:59:10.6	15.312	0.001	16.947	0.003	17.753	0.011	3	...
1009	...	2:26:38.45	61:59:26.2	18.138	0.013	19.585	0.028	20.080	0.120	2	...
1010	...	2:26:40.83	61:58:11.7	17.233	0.005	18.736	0.011	18.000	0.023	3	...
1011	...	2:26:34.54	61:58:16.6	18.124	0.013	20.069	0.042	20.883	0.235	2	...
1012	...	2:26:34.69	61:57:32.9	17.853	0.010	19.403	0.023	20.086	0.121	2	...
1013	...	2:26:35.17	61:57:11.0	16.616	0.003	17.989	0.006	18.891	0.030	3	...
1014	...	2:26:39.27	61:57:06.2	17.501	0.006	19.211	0.015	20.046	0.104	3	...
1015	93	2:26:33.94	61:56:57.2	14.739	0.001	15.757	0.001	16.043	0.003	3	...
1016	...	2:26:33.30	61:56:58.6	15.584	0.001	16.914	0.003	16.923	0.008	3	...

NOTE.—Table 2 is presented in its entirety in the electronic edition of the *Astronomical Journal*. A portion is shown here for guidance regarding its form and content.

This figure "OEY\_FIG2.jpg" is available in "jpg" format from:

<http://arxiv.org/ps/astro-ph/0501136v1>